Letter

Experimental demonstration of negative refraction of water waves using metamaterials with hyperbolic dispersion

Léo-Paul Euvé [1], Kim Pham [2], Philippe Petitjeans [1], Vincent Pagneux [3], and Agnès Maurel [4]

[1] *Laboratoire de Physique et Mécanique des Milieux Hétérogènes, ESPCI, Université PSL, CNRS, Sorbone Université, Univ. Paris Diderot, 7 Quai Saint-Bernard, 75005 Paris, France*

[2] *IMSIA, ENSTA Paris, Université Paris-Saclay, bd des Maréchaux, 91732 Palaiseau, France*

[3] *Laboratoire d'Acoustique de l'Université du Mans, Avenue Olivier Messiaen, 72085 Le Mans Cedex 9, France*

[4] *Institut Langevin, ESPCI, Université PSL, CNRS, Univ. Paris Diderot, 1 rue Jussieu, 75005 Paris, France*

(Received 12 March 2024; accepted 17 October 2024; published 12 November 2024)

In this study, we experimentally demonstrate the possibility of negative refraction of water waves, using a locally resonant metamaterial. This metamaterial exhibits a dispersion that encompasses elliptical and hyperbolic regimes, characterized by theoretical analysis and supported by experimental validation. In the frequency range associated with hyperbolic dispersion, we confirm and characterize the appearance of negative refraction. Our experimental achievement provides convincing evidence of the potential of metamaterials for water wave control.

DOI: 10.1103/PhysRevFluids.9.L112801

Veselago's pioneering work [1] laid the foundations for the exciting exploration of negative wave refraction, a phenomenon that has captured the attention of researchers for many years [2–4]. While the usual law of refraction predicts that, as a ray passes from one medium to another, the incident and refracted rays lie on opposite sides of normal at the point of incidence, negative refraction defies this law by producing incident and refracted rays on the same side of the normal. This intriguing property has paved the way for innovative wave manipulation, offering potential applications across various wave domains, from optics [5,6] to acoustics [7,8]. A promising approach to achieving negative refraction is based on hyperbolic dispersion [9,10], departing from the traditional idea stemming from Veselago's work, which involved elliptical dispersion with double negativity. Materials characterized by hyperbolic dispersion exhibit unusual optical or acoustic properties, where refractive index curves take the form of hyperbolic branches rather than circles or ellipses. Although the importance of hyperbolic metamaterials as a tool for controlling waves is substantial and has been demonstrated experimentally in acoustics [11–13] and in elastodynamics [14,15], the realization of a truly hyperbolic metamaterial for water waves has not been reported so far.

In this Letter, we present a detailed study focused on designing and characterizing a metamaterial capable of inducing negative refraction of water waves. Our metamaterial is crafted using an array of subwavelength resonators inspired by Helmholtz acoustic resonators [16,17]. This innovative approach endows the metamaterial with highly anisotropic dispersion properties that span both elliptical and hyperbolic regimes, with negative refraction being observable in the hyperbolic regime. We provide a comprehensive experimental characterization of this metamaterial, supported by an in-depth theoretical analysis based on the Bloch-Floquet method combined with homogenization techniques developed in [18], see also [19]. Additionally, we include direct numerical simulations of the three-dimensional problem using Comsol Multiphysics.

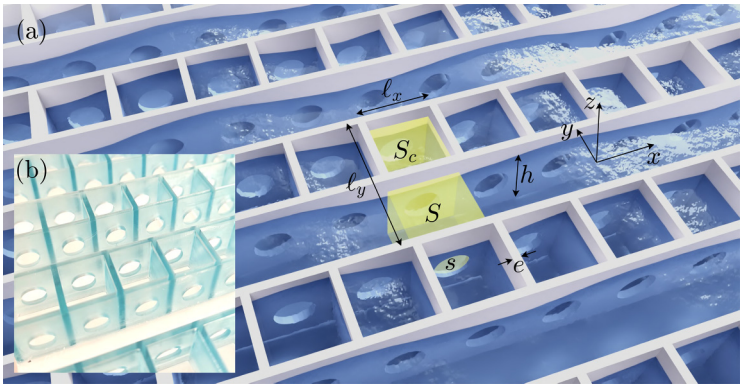

FIG. 1. (a) Conceptual view of the hyperbolic metamaterial for water waves that span elliptic and hyperbolic dispersions; (b) experimental realization of the metamaterial structure, built thanks to a 3D printer.

The resonant metamaterials is shown in Fig. 1. It consists of alternating open channels and resonant channels, formed by an array of resonators whose vertical walls extend through the entire water depth $h = 2\,\mathrm{cm}$. The three-dimensional unit cell is $\ell_x \times \ell_y \times h$, with $\ell_x = \ell = 2\,\mathrm{cm}$ and $\ell_y = 2\ell$; it consists of a single resonator and a part of the open canal, with horizontal cross sections $S_\mathrm{c} = 1.8^2\ \mathrm{cm}^2$ and $S = 1.8 \times 2\ \mathrm{cm}^2$, respectively. The resonant cavities communicate with the adjacent open canals through submerged circular holes drilled in two opposite walls and centered at $z = -h/2$. These holes have a cross-sectional area $s = \pi\, 0.5^2\ \mathrm{cm}^2$ and a length $e = 0.2\,\mathrm{cm}$, which corresponds to the thickness of the wall. The design of this device, which enables negative refraction, is based on the model introduced in [18]. In essence, the model analyzes the complete three-dimensional problem in the harmonic regime with time dependence $e^{-i\omega t}$, where $\omega = 2\pi f$ and f represents the operating frequency. In this regime, the velocity potential $\varphi(\boldsymbol{r})$, where $\boldsymbol{r} = (x, y, z)$, within an inviscid, incompressible water column exhibiting irrotational motion, satisfies Laplace's equation, supplemented by boundary conditions at the free surface $z = 0$ (with z oriented vertically upwards) and at the rigid wall boundaries, denoted by w, specifically

$$\Delta\varphi(\boldsymbol{r}) = 0, \quad \frac{\partial\varphi}{\partial z}(x, y, 0) = \frac{\omega^2}{g}\varphi(x, y, 0), \quad \nabla\varphi \cdot \boldsymbol{n}_{|\mathrm{w}} = 0, \tag{1}$$

where g is the gravitational constant and $\boldsymbol{n}$ is the local normal to the walls, including the resonator walls and the sea bottom at $z = -h$. The model assumes a subwavelength regime, indicating that the wavelength corresponding to the wave number k, which satisfies the dispersion relation in a water column of depth h as described by

$$\omega^2 = gk\tanh(kh), \tag{2}$$

is significantly greater than the dimension ℓ of the unit cell. Through the combination of Bloch-Floquet analysis with asymptotic homogenization (see Appendix A), the dispersion $\boldsymbol{\kappa}(\omega)$ for this metamaterial was derived in the following form:

$$h_x\kappa_x^2 + h_y\kappa_y^2\,\mathrm{sinc}^2\frac{\kappa_y\ell_y}{2} = \frac{\omega^2}{g_\mathrm{e}}, \quad h_x = \frac{\tanh(kh)}{k}, \quad h_y = \frac{\alpha^2\gamma}{1-\Omega^2}\,h, \quad g_\mathrm{e} = \frac{1-\Omega^2}{1+\gamma-\Omega^2}\,g, \tag{3}$$

where $\mathrm{sinc}x = \sin x/x$, $\gamma = S_\mathrm{c}/S$ is a constant nondimensional parameter, and both Ω and α are nondimensional frequency-dependent parameters with

$$\Omega = \frac{\omega}{F(kh)}, \quad \alpha = \frac{F(kh)\ell_y}{2\sqrt{gh}}, \tag{4}$$

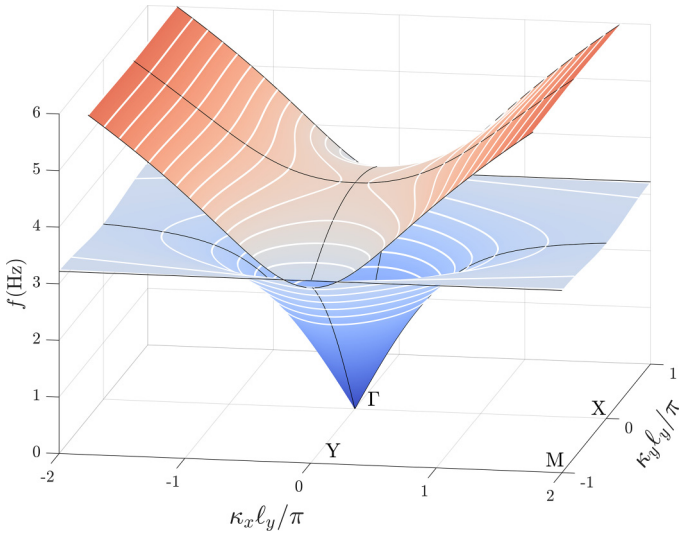

FIG. 2. Theoretical full band structure $\boldsymbol{\kappa} = (\kappa_x, \kappa_y)$ as a function of frequency $f = \omega/(2\pi)$, from (3). The white lines show isofrequency contours at the working frequencies, the black lines show the dispersion along ΓX, ΓY, and YM.

and $F(kh) = 2\pi f_{\mathrm{sw}} \sqrt{\cosh(kh/2)/\cosh(kh)}$. The resonance frequency of a single cavity is at $\omega = 2\pi f_0$ realizing $\Omega = 1$ and accordingly, f_0 tends to f_{sw} in the shallow water limit, see (A2) in Appendix A.

The cavities were built using a 3D printer with a resin material that allows the menisci to slide smoothly along the walls. We measured the resonance frequency of a single cavity at $f_0 = 3.22$ Hz, corresponding to $f_{\mathrm{sw}} = 3.83$ Hz, which matches the numerical value and is close to the theoretical value of $f_{\mathrm{sw}} = 3.18$ Hz. Figure 2 presents the theoretical full band structure (κ_x, κ_y) from (3) as a function of frequency, revealing elliptic dispersion for $f < f_0$ ($h_y > 0$) and hyperbolic dispersion otherwise ($h_y < 0$). It is noteworthy that, at low frequencies, the metamaterial already exhibits a degree of anisotropy, albeit moderate, with $h_y/h_x \to \alpha^2\gamma \sim 1.1$. In contrast, at higher frequency, anisotropy becomes very pronounced, with $h_y/h_x \to 0$. In this latter case, propagation is allowed only along the x direction, meaning that the resonant canal behaves as a plain block with $\kappa_x = k$ satisfying (2) [18,20,21]. Finally, we observe a flat branch at resonance $f = f_0$ along YM, corresponding to a localized mode characterized by arbitrary amplitude in a resonant cavity and zero amplitude in the open channels (see Appendix A).

To experimentally characterize the anisotropy of water waves over our metamaterial, we use a point source generated by a linear motor equipped with a fine tip that moves vertically in a sinusoidal motion. Two sets of experiments are conducted, with the source positioned either inside or outside a resonator. For each experiment, wave fields are measured using an optical method known as Fourier Transform Profilometry (FTP, see Appendix B), which provides spatially and temporally resolved measurements of the free surface elevation $\eta(x, y, t)$ [22–24]. Measurements are taken in a 36×36 cm^2 area with a spatial resolution of 0.35 mm; the temporal resolution, determined by the camera's frame rate, is 1/50 s. The fields $\eta(x, y, t)$ are measured for a source frequency f over a duration of 20 periods, resulting in the complex fields $\eta(x, y, f)$ through a time Fourier transform. Figure 3(a) shows typical measurements of $\eta(x, y, f)$ in real space (x, y), and Fig. 3(b) presents their 2D spatial Fourier transforms $\eta(\kappa_x, \kappa_y, f)$. In these latter fields, the white lines correspond to the theoretically predicted isofrequency contours, showing very good qualitative agreement.

These measurements were carried out for 22 values of f in the range of $(2, 6)$ Hz to obtain the experimental dispersion curves along the main directions of the Brillouin zone. Specifically,

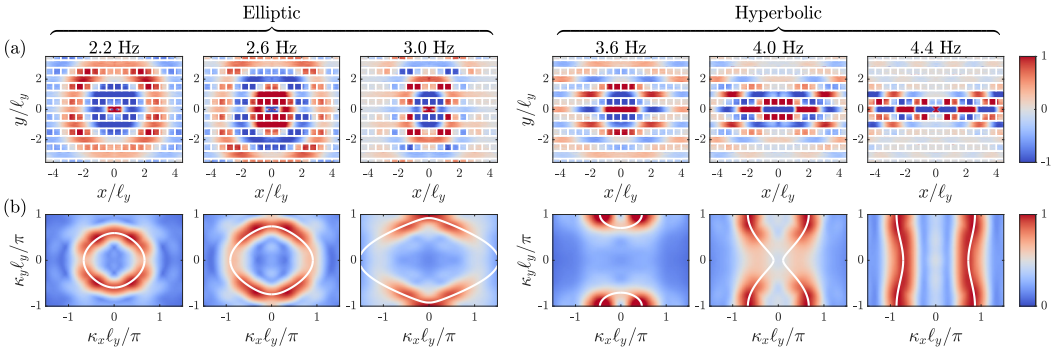

FIG. 3. (a) FTP measurements of free-surface elevation $\eta(x, y, f)$ for a point source emitting at frequency f in the anisotropic metamaterial. (b) Experimental dispersion by means of $\eta(\kappa_x, \kappa_y, f)$ (red regions) obtained by 2D spatial Fourier transforms of the fields in (a). The solid white lines show the theoretical dispersion, according to (3); all fields are normalized to their maximum.

for each frequency, we extracted the value of κ_y for $\kappa_x = 0$ (ΓY direction) and the value of κ_x for $\kappa_y = 0$ and $\kappa_y = \pi/\ell_y$ (ΓX, YM directions). The results are shown in Fig. 4 (symbols), along with the theoretical prediction from (3) (using $f_{\mathrm{sw}} = 3.83\,\mathrm{Hz}$ as before) and the numerical results obtained by solving the 3D problem in the unit cell, as described in [18]. The overall agreement between the experiments, theory, and numerical simulations is good, although a loss of accuracy is observed at the higher frequencies. This discrepancy can be attributed to surface tension, neglected in the model and 3D numerical simulations, which increases the wavelength of propagating modes in open channels, as it would in an open area. As expected, the flat branch along YM is not observed experimentally, as it is associated with a mode confined within a single resonator. It should also be noted that the model does not account for the avoided crossing between the two branches.

We now turn our attention to the potential for negative refraction in the structure. As can already be seen from the results in Fig. 4, the group velocity $\partial\omega/\partial\kappa_y$ is negative on the hyperbolic branch along ΓY, a phenomenon also visible in the isofrequency contours of Fig. 3(b) for $f \geqslant 3.6\,\mathrm{Hz}$. Along this branch, near the Γ point, κ_y approaches zero, allowing us to unambiguously state, using

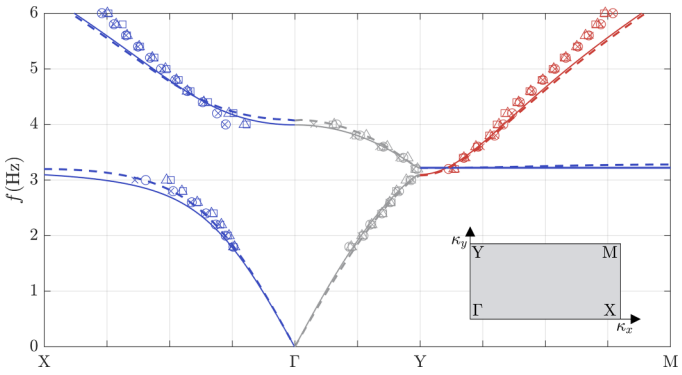

FIG. 4. Dispersion in the principal directions of the Brillouin zone. Solid lines show the theoretical dispersion (3) using $f_{\mathrm{sw}} = 3.83\,\mathrm{Hz}$, symbols the experimental dispersion (for four sets of experiments), and dashed lines correspond to numerical simulations of the three-dimensional problem. Along YM, the model does not account for avoided crossing between the two branches.

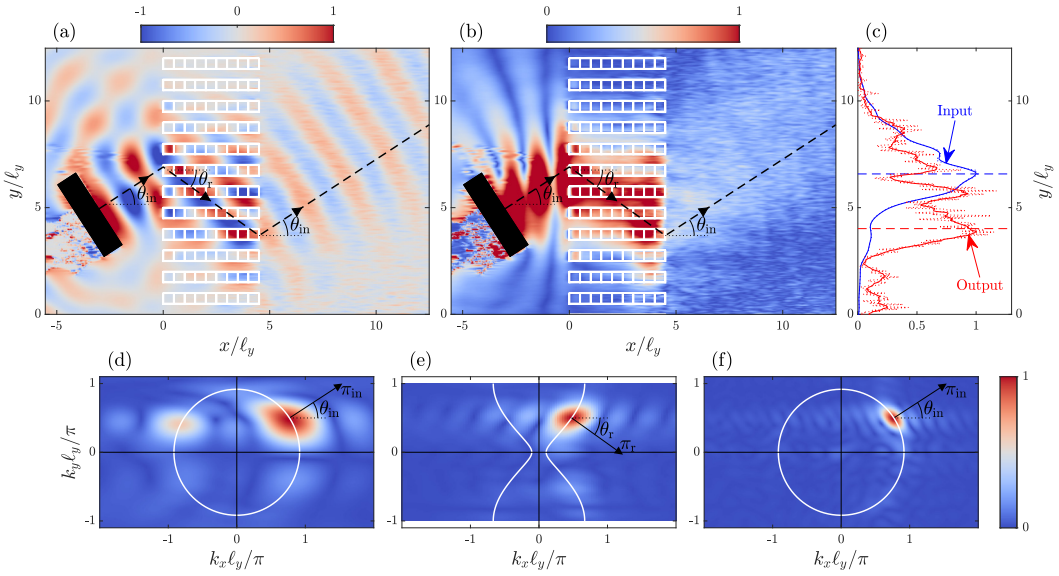

FIG. 5. Experimental evidence of negative refraction–(a), (b) FTP measurements of the surface elevation $\eta(x, y, f)$ (real part and modulus) for an incident beam at an incidence $\theta_{in} = 31^\circ$, showing negative refraction within the metamaterial slab ($\theta_r = -33^\circ$) and emerging at $x = L = 9\ell$ ($f = 4$ Hz). The fields are presented with loss compensation; see Appendix B. (c) Normalized wave amplitudes $|\eta(x, y, f)|^2$ at $x = -\ell$ (blue) and $x = L + \ell$ (red). Solid curves represent data smoothing (dotted lines), and vertical dashed lines indicate the theoretical positions of the centers of the incoming (blue) and outgoing (red) beams. (d), (e), (f) 2D spatial Fourier transforms of $\eta(x, y, f)$ for (d) $x < 0$, (e) $0 < x < L$ and (f) $x > L$. In each panel, the solid white lines represent the theoretical dispersion (2) or (3), and Poynting vector $\boldsymbol{\pi}_{in}$, from (6), or $\boldsymbol{\pi}_r$, from (5).

(3) with $\mathrm{sinc}\kappa_y\ell_y/2 \simeq 1$, that the Poynting vector inside the metamaterial takes the form

$$\boldsymbol{\pi}_r = 2\omega|\varphi|^2(h_x\kappa_x\boldsymbol{e}_x + h_y\kappa_y\boldsymbol{e}_y), \tag{5}$$

while in the free water it is described by

$$\boldsymbol{\pi}_{in} = 2\omega|\varphi^{in}|^2 h(k_x\boldsymbol{e}_x + k_y\boldsymbol{e}_y), \tag{6}$$

with $k = \sqrt{k_x^2 + k_y^2}$ satisfying (2). As a result, for an incident wave in free water with $k_x, k_y > 0$ striking an interface with the metamaterial region, our model indeed predicts negative refraction for $\omega > 2\pi f_0$, where $h_y < 0$ since the sign of the y component of the Poynting vector changes. Experimentally, this negative refraction was investigated by directing a wave beam at a frequency of $f = 4$ Hz onto a metamaterial slab 9ℓ (18 cm) long, placed in a $30\ell \times 80\ell$ (1.6×0.6 m^2) tank. The incident beam was generated by an oscillating plate inclined at an angle $\theta = 31^\circ$, producing a refraction angle $\theta_r \simeq -33^\circ$, small enough to minimize the wave attenuation due to propagation through the metamaterial. The fields shown in Figs. 5(a) and 5(b) correspond to the results obtained in real space (x, y) (in real part and magnitude, respectively). To clearly visualize the negative refraction, losses were compensated (see Appendix B). The dashed lines indicate the path predicted by the model, according to (5) and (6), in good agreement with the measurements. Figures 5(d)–5(f) display the two-dimensional spatial Fourier transforms inside and outside the metamaterial slab. Outside the metamaterial, in the (k_x, k_y) plane [panels (d) and (f)], the energy maximum (red zone) corresponds to the value of $\boldsymbol{k}$, parallel to $\boldsymbol{\pi}_{in}$ as given by (6). It should be noted that in panel (d), the presence of a maximum at $(-k_x, k_y)$ indicates reflection by the metamaterial, quantified at approximately 60%, indicating an impedance mismatch between the two media. Inside the metamaterial, in the (κ_x, κ_y) plane [panel (e)], the energy maximum yields the wave vector $\boldsymbol{\kappa}$,

which closely aligns with the theoretical dispersion (3). In this region, $\boldsymbol{\kappa}$ is not parallel to $\boldsymbol{\pi}_r$, which represents the trajectory of the energy flux observed in panels (a) and (b).

In conclusion, the application of metamaterial concept to surface water waves has led to innovative advancements in control [25–28], attenuation [29,30], and amplification [31], as well as the realization of negative elliptical dispersion [32,33]. In this study, we present for the first time a metamaterial that spans both elliptical and hyperbolic dispersion regimes, and we provide experimental validation of negative refraction in the hyperbolic regime.

Acknowledgments. The authors acknowledge the support of the ANR under Grants No. ANR-21-CE30-0046 CoProMM and No. ANR-19-CE08-0006 MetaReso.

Appendix A: Additional information on the model. The model in [18] analyzes the relationship satisfied within the unit cell by the velocity potentials in a single resonator and in a part of the adjacent open channel. According to Bloch-Floquet theory, these are denoted $\varphi(\boldsymbol{r}) = \varphi_r e^{i\boldsymbol{\kappa r}}$ and $\varphi(\boldsymbol{r}) = \varphi_a e^{i\boldsymbol{\kappa r}}$, respectively, where (φ_r, φ_a) are constants that satisfy the relations

$$(\Omega^2 - 1)\varphi_r + \frac{1}{2}(1 + e^{i\kappa_y \ell_y})\varphi_a = 0, \quad \frac{\gamma}{2}(1 + e^{-i\kappa_y \ell_y})\varphi_r + \left(\Omega^2 - \gamma - \frac{g h_x \kappa_x^2}{F^2(kh)}\right)\varphi_a = 0, \tag{A1}$$

(see (E3–E4) in [18]). The solvability condition of (A1) yields the dispersion (3). However, when $\kappa_y \ell_y = \pm\pi$, (A1) predicts the existence of a flat branch at $\Omega = 1$, associated with a compact localized mode, where $\varphi_a = 0$ and φ_r can take any arbitrary value [34].

In the model developed in [18], the resonance frequency f_{sw} in the shallow water limit is derived by integrating the Laplace equation within a resonant cavity, while accounting for boundary conditions at the free surface and at the walls. This yields

$$(2\pi f_{sw})^2 = \frac{2gs}{S_c e_{eff}}, \tag{A2}$$

where $e_{eff} = e + \epsilon\sqrt{s}$ represents an effective length. The dimensionless parameter ϵ is determined by solving the problem of a perfect fluid flowing though a hole of unitary section; for a circular hole, $\epsilon = 1.12$ resulting in $f_{sw} = 3.18$ Hz, in agreement with 3D numerical simulation.

As mentioned earlier, the cavities were fabricated using a 3D printer with a resin material designed to ensure smooth sliding of the menisci along the walls. This approach allowed us to confirm that the piston mode within the cavities is observed without the influence of surface tension. The discrepancy between the resonant frequency, measured experimentally and numerically, $f_{sw} = 3.83$ Hz and the theoretical value $f_{sw} = 3.18$ Hz, is due to the circular holes not being very small compared to the cavity dimensions, as assumed in theory.

Appendix B: Additional information on the experiments. Wave field measurements are performed using the Fourier Transform Profilometry (FTP) method [22,23]. This technique involves projecting a fringe pattern onto the free surface of the water, which is then captured by a camera (see Fig. 6). To enhance the diffusivity of the free surface, white dye is added to the water, which does not affect the hydrodynamic properties of the water [24]. The deformed fringe pattern caused by the wave propagation is compared to the original pattern (water at rest), allowing the generation of a phase map from which the free surface elevation can be reconstructed.

The experimental set-up, illustrated in Fig. 6, involves conducting experiments in a water tank measuring 1.6 m in length and 0.6 m in width. Two inclined beaches, each with a 5° slope, are positioned at both ends of the tank to prevent unwanted reflections. For the negative refraction experiments, the metamaterial slab is centrally placed within the tank. The wave maker, used for the negative refraction result in Fig. 5, consists of a horizontal cylinder, 16 cm long (approximately 2 wavelengths) and 4 cm in diameter, driven by a linear motor. It is inclined relative to the y axis to produce a wave beam with a specific incident angle. To measure the experimental dispersion relation (Figs. 3 and 4), the horizontal cylinder is replaced by a fine tip to position the source inside a resonator or an open channel.

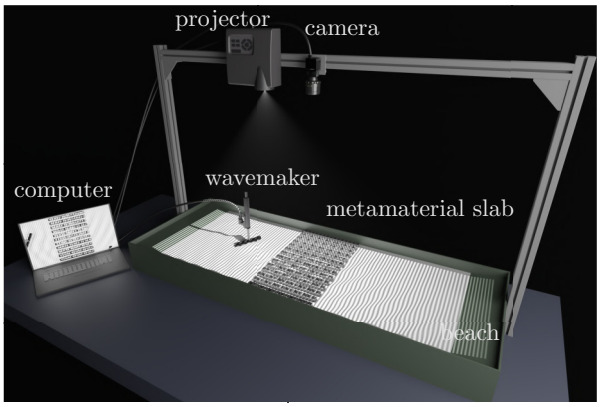

FIG. 6. Experimental setup for the negative refraction experiment, with the metamaterial slab positioned centrally within the tank, the inclined wave maker and the system projector-camera for the FTP measurements.

The fields shown in Figs. 5(a) and 5(b) are presented with loss compensation to clearly delineate the path of waves within the metamaterial, following the method described in [35]. For completeness, the original field is depicted in Fig. 7 along with its y-averaged profile (using a logarithmic scale). This representation indicates that the losses within the slab are well approximated by an exponential decay of the form $e^{-0.22|\kappa|x}$. Consequently, the loss-compensated fields displayed in Fig. 5 were obtained by normalizing the fields with $\eta(x, y) \to \eta(x, y)/V(x)$, where

$$V(x) = \begin{cases} 1, & x < 0, \\ e^{-0.22|\kappa|x}, & 0 < x < L, \\ e^{-0.22|\kappa|L}, & x > L. \end{cases} \tag{B1}$$

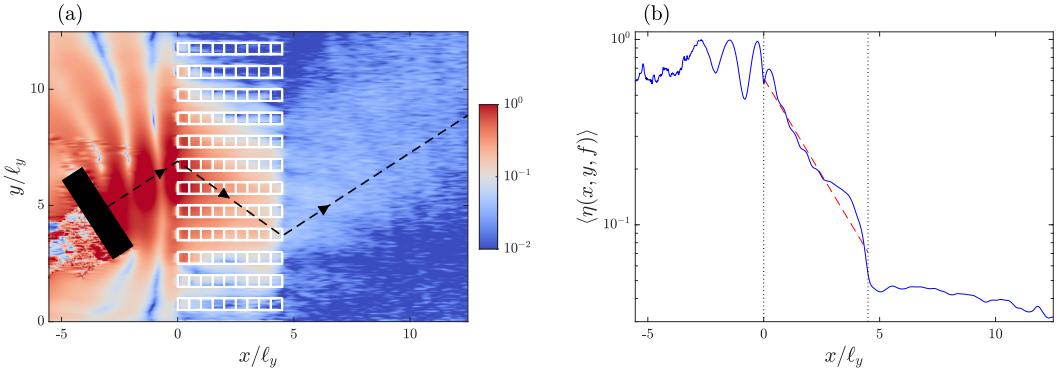

FIG. 7. (a) Original field $\eta(x, y, f)$. (b) Average of the original field along y (blue curve), fit of the losses in the metamaterial (red line), and the two vertical lines representing the position of the metamaterial.

We emphasize that the attenuation observed, due to viscous and meniscus effects, which are not accounted for in the model or the numerical simulations, is particularly significant at the scale of our laboratory experiments. This effect would diminish at larger scales.

[1] V. G. Veselago, Electrodynamics of substances with simultaneously negative ϵ and μ, Usp. Fiz. Nauk **92**, 517 (1967).

[2] D. R. Smith and N. Kroll, Negative refractive index in left-handed materials, Phys. Rev. Lett. **85**, 2933 (2000).

[3] S. Foteinopoulou, E. N. Economou, and C. M. Soukoulis, Refraction in media with a negative refractive index, Phys. Rev. Lett. **90**, 107402 (2003).

[4] D. R. Smith, J. B. Pendry, and M. C. Wiltshire, Metamaterials and negative refractive index, Science **305**, 788 (2004).

[5] J. B. Pendry, Negative refraction makes a perfect lens, Phys. Rev. Lett. **85**, 3966 (2000).

[6] G. V. Eleftheriades and K. G. Balmain, *Negative-Refraction Metamaterials: Fundamental Principles and Applications* (John Wiley & Sons, Hoboken, New Jersey, 2005).

[7] J. Christensen and F. J. G. de Abajo, Anisotropic metamaterials for full control of acoustic waves, Phys. Rev. Lett. **108**, 124301 (2012).

[8] R. V. Craster and S. Guenneau, *Acoustic Metamaterials: Negative Refraction, Imaging, Lensing and Cloaking* (Springer Science & Business Media, Dordrecht, Netherlands, 2012), Vol. 166.

[9] A. Poddubny, I. Iorsh, P. Belov, and Y. Kivshar, Hyperbolic metamaterials, Nat. Photonics **7**, 948 (2013).

[10] A. Sternbach, S. Moore, A. Rikhter, S. Zhang, R. Jing, Y. Shao, B. Kim, S. Xu, S. Liu, J. Edgar *et al.*, Negative refraction in hyperbolic hetero-bicrystals, Science **379**, 555 (2023).

[11] V. M. García-Chocano, J. Christensen, and J. Sánchez-Dehesa, Negative refraction and energy funneling by hyperbolic materials: An experimental demonstration in acoustics, Phys. Rev. Lett. **112**, 144301 (2014).

[12] C. Shen, Y. Xie, N. Sui, W. Wang, S. A. Cummer, and Y. Jing, Broadband acoustic hyperbolic metamaterial, Phys. Rev. Lett. **115**, 254301 (2015).

[13] R. E. Christiansen and O. Sigmund, Experimental validation of systematically designed acoustic hyperbolic meta material slab exhibiting negative refraction, Appl. Phys. Lett. **109**, 101905 (2016).

[14] J. H. Oh, H. Min Seung, and Y. Young Kim, A truly hyperbolic elastic metamaterial lens, Appl. Phys. Lett. **104**, 073503 (2014).

[15] H. Lee, J. H. Oh, H. M. Seung, S. H. Cho, and Y. Y. Kim, Extreme stiffness hyperbolic elastic metamaterial for total transmission subwavelength imaging, Sci. Rep. **6**, 24026 (2016).

[16] L.-P. Euvé, K. Pham, P. Petitjeans, V. Pagneux, and A. Maurel, Time domain modelling of a helmholtz resonator analogue for water waves, J. Fluid Mech. **920**, A22 (2021).

[17] L.-P. Euvé, N. Piesniewska, A. Maurel, K. Pham, P. Petitjeans, and V. Pagneux, Control of the swell by an array of helmholtz resonators, Crystals **11**, 520 (2021).

[18] L.-P. Euvé, K. Pham, and A. Maurel, Negative refraction of water waves by hyperbolic metamaterials, J. Fluid Mech. **961**, A16 (2023).

[19] J.-J. Marigo, A. Maurel, and K. Pham, Negative refraction in a single-phase flexural metamaterial with hyperbolic dispersion, J. Mech. Phys. Solids **170**, 105126 (2023).

[20] A. N. Norris and X. Su, Enhanced acoustic transmission through a slanted grating, C. R. Méc. **343**, 622 (2015).

[21] R. Porter, Plate arrays as a perfectly-transmitting negative-refraction metamaterial, Wave Motion **100**, 102673 (2021).

[22] A. Maurel, P. Cobelli, V. Pagneux, and P. Petitjeans, Experimental and theoretical inspection of the phase-to-height relation in fourier transform profilometry, Appl. Opt. **48**, 380 (2009).

[23] P. J. Cobelli, A. Maurel, V. Pagneux, and P. Petitjeans, Global measurement of water waves by fourier transform profilometry, Exp. Fluids **46**, 1037 (2009).
[24] A. Przadka, B. Cabane, V. Pagneux, A. Maurel, and P. Petitjeans, Fourier transform profilometry for water waves: how to achieve clean water attenuation with diffusive reflection at the water surface? Exp. Fluids **52**, 519 (2012).
[25] X. Hu, Y. Shen, X. Liu, R. Fu, and J. Zi, Superlensing effect in liquid surface waves, Phys. Rev. E **69**, 030201(R) (2004).
[26] C. Berraquero, A. Maurel, P. Petitjeans, and V. Pagneux, Experimental realization of a water-wave metamaterial shifter, Phys. Rev. E **88**, 051002 (2013).
[27] H. Chen, J. Yang, J. Zi, and C. T. Chan, Transformation media for linear liquid surface waves, Europhys. Lett. **85**, 24004 (2009).
[28] A. Maurel, J.-J. Marigo, P. Cobelli, P. Petitjeans, and V. Pagneux, Revisiting the anisotropy of metamaterials for water waves, Phys. Rev. B **96**, 134310 (2017).
[29] H. Kagemoto, M. Murai, M. Saito, B. Molin *et al.*, Experimental and theoretical analysis of the wave decay along a long array of vertical cylinders, J. Fluid Mech. **456**, 113 (2002).
[30] L.-P. Euvé, K. Pham, R. Porter, P. Petitjeans, V. Pagneux, and A. Maurel, Perfect resonant absorption of guided water waves by autler-townes splitting, Phys. Rev. Lett. **131**, 204002 (2023).
[31] A. J. Archer, H. A. Wolgamot, J. Orszaghova, L. G. Bennetts, M. A. Peter, and R. V. Craster, Experimental realization of broadband control of water-wave-energy amplification in chirped arrays, Phys. Rev. Fluids **5**, 062801(R) (2020).
[32] M. Farhat, S. Guenneau, S. Enoch, and A. Movchan, All-angle-negative-refraction and ultra-refraction for liquid surface waves in 2d phononic crystals, J. Comput. Appl. Math. **234**, 2011 (2010).
[33] X. Hu, C. T. Chan, K.-M. Ho, and J. Zi, Negative effective gravity in water waves by periodic resonator arrays, Phys. Rev. Lett. **106**, 174501 (2011).
[34] D. Leykam, A. Andreanov, and S. Flach, Artificial flat band systems: From lattice models to experiments, Adv. Phys.: X **3**, 1473052 (2018).
[35] N. Kaina, F. Lemoult, M. Fink, and G. Lerosey, Negative refractive index and acoustic superlens from multiple scattering in single negative metamaterials, Nature (London) **525**, 77 (2015).